The Sensitivity of Salt Wedge Estuaries to Channel Geometry

ANTHONY R. POGGIOLI AND ALEXANDER R. HORNER-DEVINE

Civil and Environmental Engineering, University of Washington, Seattle, Washington

(Manuscript received 22 October 2014, in final form 25 April 2015)

ABSTRACT

The authors develop a two-layer hydraulic model to determine the saline intrusion length in sloped and converging salt wedge estuaries. They find that the nondimensional intrusion length $L_* = C_i L/h_S$ depends significantly on the channel bottom slope and the rate and magnitude of landward width convergence, in addition to the freshwater Froude number. In the definition of L_*, C_i is a quadratic interfacial drag coefficient, L is the salt wedge intrusion length, and h_S is the depth at the mouth of the estuary. Bottom slope is found to limit the saline intrusion length, and this limitation accounts for the deviation of the observed exponent n in a scaling relationship with the river discharge of the form $L \sim Q^{-n}$ from the canonical value of 2 to 2.5 predicted by the theory of Schijf and Schönfeld for a flat, prismatic estuary. The authors find that estuary convergence is important only when the ratio of the slope-limited intrusion length to the convergence length is greater than one, and that the effects of convergence are less significant than those of slope limitation. They compare this model to field and validated numerical data and find that the solution predicts the intrusion length with good accuracy, improving on the flat, prismatic solution by orders of magnitude. While this model has good predictive capability, it is sensitive to C_i and the location of the hydraulic control point, both difficult to determine a priori.

1. Introduction

A salt wedge forms when an estuary is dominated by the stratifying influence of a freshwater inflow, in opposition to the vertically homogenizing influence of tides (Geyer and MacCready 2014). Salt wedges are characterized by strong vertical stratification confined to a narrow pycnocline, which divides a nearly fresh layer of outflowing water from the layer of ocean water beneath it (Geyer and Ralston 2011). The dynamics of this flow are described effectively by the two-layer hydraulic theory as developed by Armi (1986) and others, perhaps modified by the inclusion of bottom and/or interfacial friction as described by, for example, Schijf and Schönfeld (1953), Pratt (1986), Geyer and Farmer (1989), and Geyer and Ralston (2011). The lower layer propagates upstream under the influence of the baroclinic pressure gradient until it is arrested by an adverse net barotropic flow in the presence of variable topography and/or interfacial friction. The structure of the salt wedge varies depending on whether it is arrested by barotropic forcing or interfacial friction. The dynamics of frictionless barotropic arrest of a salt wedge in a diverging channel upstream of a constriction are described by Armi and Farmer (1986), and those of a frictionally arrested salt wedge in a prismatic channel are described by Schijf and Schönfeld (1953). Here we describe the dynamics of an arrested salt wedge under the influence of both friction and variable topography.

Schijf and Schönfeld (1953) develop an analytical theory for the structure of a frictionally arrested salt wedge in a flat channel of uniform width. They derive an explicit formula for the intrusion length (L) as a function of river discharge (Q) (a length–discharge relationship), and their model is used by Harleman (1961) to obtain an implicit expression for the shape of the intrusion. Over much of the relevant parameter space, the length–discharge relationship they derive predicts $L \sim Q^{-2}$ to $Q^{-2.5}$ (Geyer and Ralston 2011). Keulegan (1966) finds experimentally that for a flat channel of uniform width, L varies with $Q^{-2.5}$, and Harleman (1961) shows that the analytical expression he derives for the shape of the salt wedge agrees with the experimental profiles reported by Keulegan (1957).

Corresponding author address: Anthony R. Poggioli, Civil and Environmental Engineering, University of Washington, 201 More Hall, Box 352700, Seattle, WA 98195.
E-mail: apogg24@u.washington.edu

DOI: 10.1175/JPO-D-14-0218.1

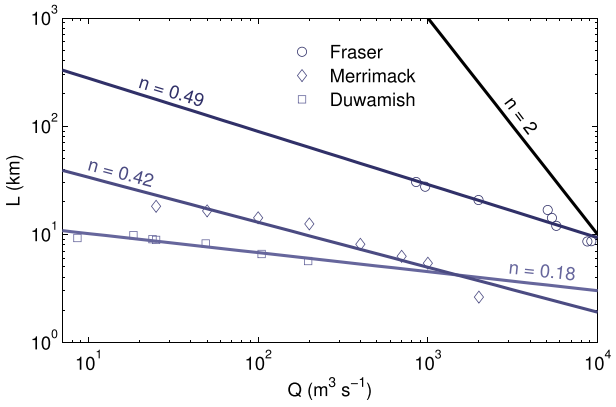

FIG. 1. Comparison of length–discharge solution for flat, prismatic estuary (Schijf and Schönfeld 1953), the $n = 2$ line, to field [Fraser, from Ward (1976), and Duwamish, from McKeon et al. (2014, manuscript submitted to *Estuaries Coasts*)] and numerical model [Merrimack, from Ralston et al. (2010)] data. Best-fit exponents for each estuary are shown.

This model thus appears to correctly describe the physics of the frictionally arrested salt wedge, at least in the absence of topographic variation. However, in real salt wedges, the dependence of L on Q, typically quantified by the exponent n in a power-law relationship of the form $L \sim Q^{-n}$, is consistently observed to be an order of magnitude smaller than the canonical values discussed above. This is illustrated in Fig. 1, which shows field [Fraser, from Ward (1976), and Duwamish, from McKeon et al. (2014, manuscript submitted to *Estuaries Coasts*)] and validated realistic numerical model [Merrimack, from Ralston et al. (2010)] data, along with the best-fit power law and corresponding exponent for each dataset. The power-law exponent varies between 0.18 and 0.49 and is always much smaller than the $n = 2$ exponent from Schijf and Schönfeld (1953). The primary goal of this work is to determine if topographic effects—in particular, a nonzero mean bottom slope and/or upstream convergence of channel width—may explain the deviation of observation from the solution for a flat, prismatic estuary due to Schijf and Schönfeld (1953).

In most estuaries, the structure of the salt wedge is strongly modified by tidal currents (e.g., Geyer and Farmer 1989). The quasi-steady arrested layer model of the salt wedge is an accurate description of the wedge at arrest, occurring soon after the upper layer begins to ebb (Geyer and Farmer 1989). The length predicted is thus an indication of the maximum intrusion. However, the arresting discharge must then be understood as the sum of the fluvial and an effective tidal discharge (Geyer and Ralston 2011). The prediction of hydraulic theory for the dependence of intrusion length on tidal amplitude as well as river discharge can only be found using a more sophisticated time-dependent model of the estuary. However, the work presented here will give a qualitative indication of the sensitivity of salt wedge length to river discharge in tidal systems, and we hope that the results will serve to indicate whether the discrepancy between observation and theory is a result of a breakdown in the assumed physics [e.g., a transition from the hydraulic to a partially mixed regime dominated by exchange flux, for which $L \sim Q^{-1/3}$ (Chatwin 1976; Monismith et al. 2002; MacCready and Banas 2011)] or an oversimplification in the application of the hydraulic equations.

In section 2, we present an overview of the theory of hydraulic descriptions of the estuary, developing equations and boundary conditions governing the structure of the two-layered arrested salt wedge, and determine the principle governing dimensionless parameters. Section 3 briefly reviews the analytical results of Schijf and Schönfeld (1953) and Harleman (1961) for the length and structure of a frictionally arrested salt wedge in a flat, prismatic channel, which is the canonical theory for the sensitivity of intrusion length to discharge to which we will compare our results. In section 4, we present the results for the dependence of intrusion length on discharge in a sloped channel of uniform width, and in section 5, we present those for the dependence of intrusion length on discharge in an exponentially converging estuary of both zero and nonzero bottom slope. In section 6, we compare our results for the dependence of intrusion length on river discharge to a numerically modeled L versus Q relationship in the Merrimack River estuary and a measured L versus Q relationship in the Duwamish River estuary (see Fig. 1) and discuss some key implications of this work.

2. Theory

Following Schijf and Schönfeld (1953), we develop a frictional two-layer hydraulic model of the salt wedge. A freshwater layer with uniform velocity varying only in the along-flow direction passes without mixing over a uniform, stationary layer of ocean water, the salt wedge. Figure 2 shows the geometry of this configuration; in general, a subscript 1 indicates a quantity in the buoyant layer, and a subscript 2 indicates a quantity in the salt wedge. We drop the subscript 1 on the velocity u because only the upper layer is flowing. Tides are not considered, and the river discharge is assumed steady. The model is one-dimensional, and the effects of lateral topographic variation on the flow are included only in the continuity equation. We

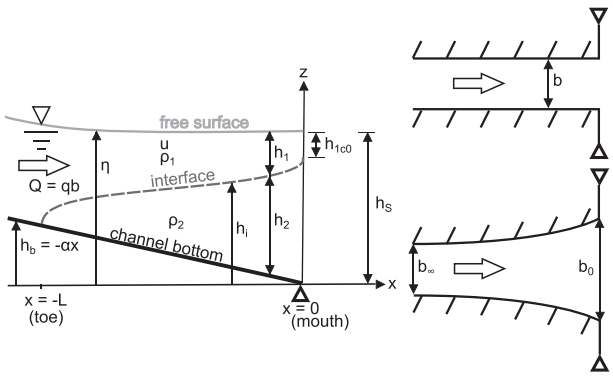

FIG. 2. (left) Side view sketch and (right) plan view sketches of model configuration. Independent and dependent model variables are shown. The plan view shows the two width configurations considered here: (top right) uniform and (bottom right) converging. The thick-lined triangles indicate hydraulic control.

parameterize the interfacial shear stress τ_i using a quadratic drag coefficient C_i that is assumed constant, such that

$$\tau_i = C_i \rho u^2, \tag{1}$$

where ρ is the density and u is the upper-layer velocity. The difference in the value of C_i depending on whether the upper- or lower-layer density is used in Eq. (1) is neglected, given the small density differences in estuarine applications. The momentum and continuity equations are

$$q \equiv \frac{Q}{b} = uh_1, \tag{2}$$

$$u\frac{du}{dx} + g\frac{d\eta}{dx} + C_i\frac{u^2}{h_1} = 0, \quad \text{and} \tag{3}$$

$$g\frac{d\eta}{dx} - g'\frac{dh_1}{dx} - C_i\frac{u^2}{h_2} = 0, \tag{4}$$

where q is the specific river discharge (volumetric discharge per unit width); Q is the river discharge; b is the channel width, assumed invariant with depth; $\eta = h_1 + h_2 + h_b$ is the free surface elevation; h_j is the thickness of the jth layer; h_b is the channel bottom elevation; g is the gravitational acceleration; $g' \equiv (\Delta\rho/\rho_2)g$ is the reduced gravitational acceleration; and $\Delta\rho \equiv \rho_2 - \rho_1$ is the density anomaly. These correspond to the equations developed by Schijf and Schönfeld (1953) with the time derivatives and lower-layer velocity set to zero and the upper-layer continuity equation integrated over x. Note that these equations apply only within the salt wedge and not upstream.

If Eqs. (2)–(4) are solved for dh_1/dx and dh_2/dx and integrated, there are numerical difficulties associated with rapidly varying topography because the gradients of the topographic variables appear explicitly. Additionally, the resulting equations become unbounded when the upper-layer internal Froude number $F_{i1} = Q/b\sqrt{g'h_1^3} = 1$. This happens at the hydraulic control, where integration begins (see section 2a). For these reasons, it is useful to combine the momentum and continuity equations and rewrite the result in terms of the buoyant hydraulic head:

$$\frac{d}{dx}\left[\frac{Q^2}{2g'b^2h_1^2} + \left(\frac{\Delta\rho}{\rho_2}\right)^{-1}\eta\right] = \frac{dH_1'}{dx} = -C_iF_{i1}^2, \quad \text{and} \tag{5}$$

$$\frac{d}{dx}\left[\left(\frac{\Delta\rho}{\rho_2}\right)^{-1}\eta - h_1\right] = \frac{dH_2'}{dx} = C_iF_{i1}^2\frac{h_1}{h_2}, \tag{6}$$

where H_j' is the buoyant hydraulic head of the jth layer. An equation eliminating the free surface slope is obtained by taking the difference of Eqs. (5) and (6):

$$\frac{d}{dx}\left(\frac{Q^2}{2g'b^2h_1^2} + h_1\right) = \frac{d\Delta H'}{dx} = -C_iF_{i1}^2\left(1 + \frac{h_1}{h_2}\right), \tag{7}$$

where here $\Delta H' \equiv H_1' - H_2'$ is termed the buoyant hydraulic head anomaly. Our solution procedure, explained in section 2c below, will be to integrate for H_1' and $\Delta H'$ and then solve for the layer thicknesses.

a. Boundary conditions

We follow Schijf and Schönfeld (1953) in assuming that the mouth is the control—that is, the flow is critical ($F_{i1}^2 = 1$) there—in the absence of varying channel topography. However, if there are significant lateral constrictions present in the estuary, the relevant control may be a channel constriction and not the river mouth. This is because flow constrictions satisfy the regularity conditions, which are necessary local topographic conditions (e.g., $db/dx = 0$) for the existence of a hydraulic control (Armi 1986).

Denoting the location of the control as $x = 0$, the first boundary condition, that $F_{i1}^2 = 1$, can be written as

$$h_1(x=0) = h_{1c}(x=0) = h_{1c0} = \left(\frac{Q^2}{b_0^2g'}\right)^{1/3}, \tag{8}$$

where h_{1c} is the critical thickness, the thickness of the upper layer when $F_{i1}^2 = 1$; h_{1c0} is the critical thickness at the control; and $b_0 = b(x = 0)$ is the channel width at the control. A second boundary condition is obtained by assuming that the total water depth at the control h_S is known:

$$\eta(x=0) = h_S. \tag{9}$$

We refer to h_S as the shoreline depth because the control is typically at the mouth, where the channel intersects the coastal shoreline. This terminology follows Lamb et al. (2012), who investigate in part the sensitivity of the shoreline depth to river discharge. We will not take into account the potential dependence of h_S on discharge here. The solutions presented in sections 3–5 assume control occurs at the estuary mouth. When comparing to data obtained in the Duwamish (see section 6b), it will be necessary to identify controls associated with lateral constrictions and occurring at locations other than the mouth.

Together, these boundary conditions are sufficient to determine the values of the upper-layer buoyant hydraulic head and hydraulic head anomaly at the control:

$$H_1'(x=0)=\frac{h_{1c0}}{2}+\left(\frac{\Delta\rho}{\rho_2}\right)^{-1}h_S=\frac{1}{2}\left(\frac{Q^2}{b_0^2g'}\right)^{1/3}+\left(\frac{\Delta\rho}{\rho_2}\right)^{-1}h_S, \tag{10}$$

and

$$\Delta H'(x=0)=\frac{3}{2}h_{1c0}=\frac{3}{2}\left(\frac{Q^2}{b_0^2g'}\right)^{1/3}. \tag{11}$$

b. Nondimensionalization of governing equations

We now nondimensionalize Eqs. (5) and (7) and boundary conditions from Eqs. (8)–(11). This will elucidate the governing dimensionless parameters and simplify the solution of this system of equations.

We nondimensionalize all vertical length scales using the total water depth at the control, h_S. We will eliminate the free surface elevation η in favor of h_1 and h_2 using the general relation $\eta = h_1 + h_2 + h_b$. We do this to reduce the number of dependent hydraulic variables to two: h_1 and h_2. We nondimensionalize all horizontal length scales by the so-called friction length h_S/C_i (Geyer and Ralston 2011), the buoyant hydraulic heads by the critical depth at the control h_{1c0}, and the channel width b by the width at the control b_0. We denote dimensionless variables by a subscript *. A list of the dimensional and corresponding nondimensional independent and dependent model variables is shown in Table 1. This procedure results in the following equations:

$$H_{1*}'=\frac{1}{2}\frac{F_f^{4/3}}{b_*^2h_{1*}^2}+\frac{1}{F_f^{2/3}}\left(\frac{\Delta\rho}{\rho_2}\right)^{-1}(h_{1*}+h_{2*}+h_{b*}), \tag{12}$$

$$\Delta H_*'=\frac{1}{2}\frac{F_f^{4/3}}{b_*^2h_{1*}^2}+\frac{h_{1*}}{F_f^{2/3}}, \tag{13}$$

$$\frac{dH_{1*}'}{dx_*}=-\frac{F_f^{4/3}}{b_*^2h_{1*}^3}, \tag{14}$$

TABLE 1. Dimensional variables and their dimensionless equivalents. The subscript j indicates that the corresponding quantity for both layers 1 and 2 are nondimensionalized in the same manner.

Dimensional variables	Nondimensional variables and definitions
x	$x_*=C_ix/h_S$
b	$b_*=b/b_0$
h_b	$h_{b*}=h_b/h_S=-(\alpha/C_i)x_*$
Q	$F_f=Q/b\sqrt{g'h_S^3}$
η	$\eta_*=\eta/h_S$
h_j	$h_{j*}=h_j/h_S$
H_j'	$H_{j*}'=H_j'/h_{1c0}$

$$\frac{d\Delta H_*'}{dx_*}=-\frac{F_f^{4/3}}{b_*^2h_{1*}^3}\left(1+\frac{h_{1*}}{h_{2*}}\right), \tag{15}$$

$$h_{1*}(x_*=0)=F_f^{2/3}, \tag{16}$$

$$h_{1*}(x_*=0)+h_{2*}(x_*=0)=1, \tag{17}$$

$$H_{1*}'(x_*=0)=\frac{1}{2}+\frac{1}{F_f^{2/3}}\left(\frac{\Delta\rho}{\rho_2}\right)^{-1}, \quad \text{and} \tag{18}$$

$$\Delta H_*'(x_*=0)=\frac{3}{2}. \tag{19}$$

We have defined the freshwater Froude number $F_f = Q/b_0\sqrt{g'h_S^3} = (h_{1c0}/h_S)^{3/2}$ (Geyer and Ralston 2011). This number is equivalent to the nondimensional net barotropic flow U_0 discussed in Armi (1986) and Armi and Farmer (1986); it is the key dynamical parameter governing two-layer hydraulic flow.

By examining Eqs. (12)–(19), we conclude that the solution is in general a function of F_f, $\Delta\rho/\rho_2$, $b_*(x_*)$, and $h_{b*}(x_*)$. In sections 4 and 5, when we investigate the behavior of this model in simple topographies, we will derive explicit geometric parameters that influence the solution.

c. Solution methodology

The simplified geometry of the model domain is specified by an assumed topography, characterized by the nondimensional channel bottom elevation and channel width as functions of x_*. Boundary conditions [Eqs. (16)–(19)] are applied at the control (assumed in sections 3–5 to be the mouth), and Eqs. (14) and (15) are numerically integrated landward from the control using a second-order method. At each step we solve Eq. (13) for h_{1*} and then solve for h_{2*} by using Eq. (12). When solving for h_{1*}, we choose the subcritical root because a supercritical solution would correspond to an upper-layer thickness that decreases landward and therefore to an infinitely long salt wedge. We integrate until the point $x_* = -L_*$, where

$h_{2*} = 0$ and the interface therefore intersects with the channel bottom. The term $L_* = C_i L/h_S$ is the nondimensional intrusion or salt wedge length.

3. Solution for a flat estuary of uniform width

Before exploring the results of this model in nonuniform topographies, it is useful to rederive the results of Schijf and Schönfeld (1953) and Harleman (1961) for the shape and length of the salt wedge in a flat estuary of uniform width, since this is the canonical theory describing the structure of an arrested salt wedge. The above authors apply the rigid lid approximation, assuming that the along-estuary variation in the free surface elevation is negligible in the friction terms. However, the free surface slope term is not explicitly set to zero; this would produce inconsistent results if applied to the individual-layer momentum equations. Rather, an equation eliminating the free surface slope must be obtained by taking the difference of the momentum equations before the rigid lid approximation can be applied.

To apply the rigid lid approximation, $h_{1*} + h_{2*} + h_{b*} = 1$, we must start with Eq. (15) because it was obtained by taking the difference of the momentum equations. We insert Eq. (13) into Eq. (15), eliminate h_{2*} by applying the rigid lid approximation, and insert $h_{b*} = 0$ and $b_* = 1$, since the estuary is assumed to be flat and prismatic. After rearranging the result, we obtain

$$(1 - h_{1*})\left(\frac{h_{1*}^3}{F_f^2} - 1\right)\frac{dh_{1*}}{dx_*} + 1 = 0. \tag{20}$$

To obtain an explicit expression for the intrusion length, we integrate Eq. (20), using boundary condition Eq. (16) and the fact that at the toe $x_* = -L_*$ and $h_{1*} = 1$:

$$\int_1^{F_f^{2/3}} (1 - h_{1*})\left(\frac{h_{1*}^3}{F_f^2} - 1\right) dh_{1*} + \int_{-L_*}^{0} dx_* = 0$$

$$\Rightarrow L_* = -\frac{1}{20}(6F_f^{4/3} - 15F_f^{2/3} - F_f^{-2} + 10). \tag{21}$$

Equation (21) is equivalent to the expressions derived by Schijf and Schönfeld (1953) and Harleman (1961, Eq. 26.22). It can be approximated by a power law of the form $L \sim Q^{-n}$, where n is always ≥2 and is <2.5 over most of the relevant parameter space. These power laws are often cited in the literature (e.g., Lerczak et al. 2009; Geyer and Ralston 2011). This solution and these power laws are shown in Fig. 3a. As noted earlier, however, n is observed to be an order of magnitude smaller in real systems, suggesting that the solution does not account

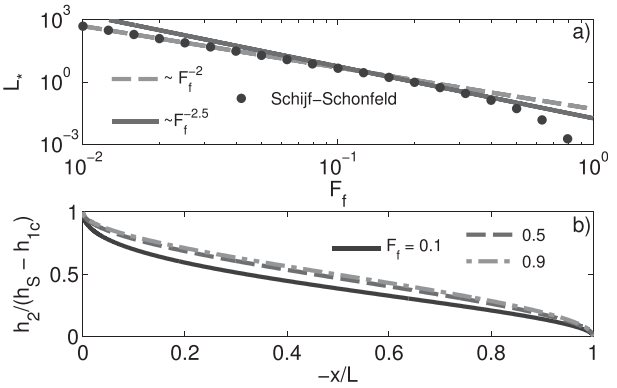

FIG. 3. (a) Nondimensional intrusion length L_* vs freshwater Froude number F_f for a flat estuary of uniform width (Schijf and Schönfeld 1953). The $L_* \sim F_f^{-2}$ and $F_f^{-2.5}$ lines are also plotted. (b) Normalized salt wedge shape (Harleman 1961) for several values of F_f.

for all of the relevant physics. An implicit expression for the shape of the salt wedge is derived by integrating from either the toe or the mouth to an arbitrary point (x_*, h_{1*}):

$$\int_1^{h_{1*}} (1 - h_{1*})\left(\frac{h_{1*}^3}{F_f^2} - 1\right) dh_{1*} + \int_{-L_*}^{x_*} dx_* = 0 \Rightarrow \frac{1}{20}F_f^{-2}(5h_{1*}^4 - 4h_{1*}^5 - 1) + \frac{1}{2}(h_{1*}^2 + 1) - h_{1*} + x_* + L_* = 0. \tag{22}$$

This is equivalent to the expression derived by Harleman (1961, Eq. 26.21). The shape of the intrusion is plotted in Fig. 3b. The figure shows the salt wedge thickness normalized by the maximum thickness at the mouth, $h_2/(h_S - h_{1c0}) = (1 - h_{1*})/(1 - F_f^{2/3})$, versus $-x_*/L_* = -x/L$ for several values of F_f. The freshwater Froude number is constrained to be between zero and one; a value of $F_f > 1$ corresponds to a critical depth that is greater than the total water depth, in which case the salt wedge is completely expelled from the channel.

We noted above that, in addition to F_f, the solution is also a function of the nondimensional density anomaly $\Delta\rho/\rho_2$. However, this parameter vanishes when we make the rigid lid approximation. It can be shown that $d\eta/dx \sim O(C_i\Delta\rho/\rho_2)$, whereas $dh_1/dx \sim O(C_i)$ in the bulk of the salt wedge. Because $\Delta\rho/\rho_2$ is on the order of 0.01, this suggests that the change in upper-layer thickness is dominated by the change in interface height, and therefore that neglecting changes in free surface elevation when calculating layer depths in the friction term is a good approximation. We anticipate that free surface

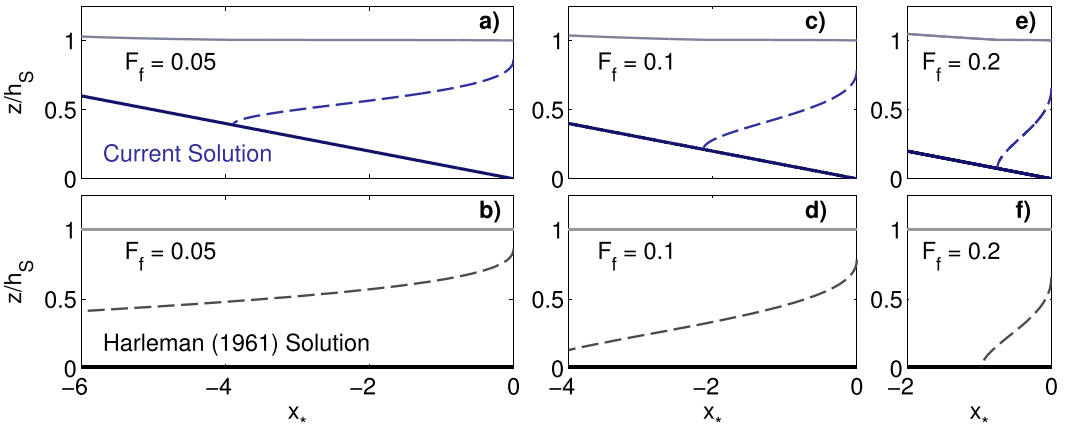

FIG. 4. Comparison of interface profile with Harleman (1961) flat bottom solution. (a),(c),(e) Three example model runs with increasing freshwater Froude number in a sloped estuary of uniform width. The dashed purple, solid purple, and gray lines correspond to the density interface, channel bottom, and free surface, respectively. (b),(d),(f) The Harleman (1961) solution for a flat estuary with a rigid lid for the same freshwater Froude numbers. The dashed gray, solid black, and solid gray lines again correspond to the density interface, channel bottom, and free surface, respectively. The horizontal dimension of each column is scaled with the distance shown on the x axis.

effects will only become important for large values of $\Delta\rho/\rho_2$. We test this hypothesis by comparing a solution of Eqs. (14) and (15) for a flat estuary, which include all free surface effects, to Eq. (21), which neglects free surface effects, for values of $\Delta\rho/\rho_2$ ranging from 0.001 to 0.025. This corresponds to a salinity difference ranging from 1.3 to 33.3 psu. The solution incorporating the influence of the changing free surface elevation on the layer thicknesses consistently predicted values of the intrusion length larger than the rigid lid solution of Schijf and Schönfeld (1953); however, the largest difference was less than 4% over this parameter range. Therefore, the differences due to free surface effects are of secondary importance compared with those resulting from the bottom slope and width variation (sections 4 and 5), which result in predictions for L_* that deviate from Schijf and Schönfeld (1953) by orders of magnitude. In these sections, we will ignore variation in $\Delta\rho/\rho_2$ in order to simplify our calculations and reduce the parameter space. We will assume a typical value of 0.02 corresponding to a salinity difference of 26.5 psu.

4. Solution for a sloped estuary of uniform width

In this section, we present the solution for the length–discharge relationship in a channel of uniform width and mean bottom slope α (see Fig. 2). In this case, because the channel bottom elevation varies with x_*, it is not possible to explicitly solve a separable equation as we did for the flat, prismatic estuary, even if the rigid lid approximation is made. We therefore integrate Eqs. (14) and (15) numerically. In Fig. 4 we present a comparison of the interface height predicted with the current solution with a sloped channel bottom ($C_i/\alpha = 10$) to that predicted by the Schijf and Schönfeld (1953) and Harleman (1961) solution for a flat estuary with the rigid lid approximation. The comparison illustrates that the bottom slope has a dynamic effect on the salt wedge (modifying the baroclinic pressure gradient and interfacial friction, see section 6a), which significantly reduces the intrusion length relative to the flat bottom solution. We also observe that the discrepancy between the two solutions decreases as the river discharge increases. At the highest F_f, the intrusion lengths are close to equal, although differences in the interface and water surface profiles are evident (Figs. 4e,f). The free surface profile upstream of the salt wedge is predicted using a typical open-channel-flow hydraulic model (see, e.g., Chow 1959).

The assumed channel bottom elevation has the form $h_b = -\alpha x$. Applying the above nondimensionalization to this expression produces $h_{b*} = -(\alpha/C_i)x_*$. This introduces a new variable into the dependence, C_i/α, which is the nondimensional value of the slope-limited maximum intrusion length. Unlike the flat estuary case, in which the salt wedge may penetrate arbitrarily far upstream in the limit of small discharge, the intrusion in a sloped estuary is slope limited as Q decreases. As $Q \to 0$ and the upper-layer thickness at the mouth $[h_{1c0} = (q^2/g')^{1/3}]$ shrinks so that the initial wedge thickness approaches h_S, the intrusion length approaches a slope-limited value of h_S/α and L_* approaches C_i/α. This mechanism is discussed in detail in section 6a and illustrated schematically in Fig. 10a. We therefore anticipate that the family of $L_*(F_f)$ curves will branch depending on this limiting value of L_*,

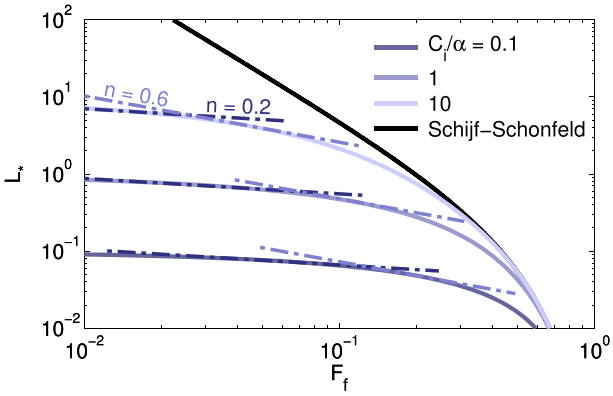

FIG. 5. Intrusion length in a channel of uniform width and nonzero mean bottom slope α. The curves are segregated by the value of the parameter C_i/α. The flat estuary solution (Schijf and Schönfeld 1953) is also shown. This corresponds to the limit $C_i/\alpha \to \infty$. Also shown are the $n = 0.2$ and 0.6 tangent lines.

with the difference between curves becoming more pronounced as F_f becomes smaller and the limiting values of L_* are approached. This is observed in Fig. 5, where we plot three L_* versus F_f solution curves for $C_i/\alpha = 0.1$, 1, 10, along with the Schijf and Schönfeld (1953) solution, which corresponds to a flat bed and therefore the limit $C_i/\alpha \to \infty$. Figure 5 confirms that L_* is a function of F_f, and C_i/α.

The value of the exponent n in Fig. 5 corresponds to the slope of these curves because they are plotted in logarithmic space. We note from the discrepancy in slope between the Schijf and Schönfeld (1953) curve and those corresponding to finite values of C_i/α the strong dependence of n on C_i/α and therefore the mean bottom slope α. Also shown in Fig. 5 are tangent lines corresponding to $n = 0.2$ and $n = 0.6$. These values of n were selected because they correspond approximately to the lower and upper limits reported in the literature (Ralston et al. 2010; McKeon et al. 2014, manuscript submitted to *Estuaries Coasts*). The value of n predicted by the model is within the range observed in the field roughly for $0.01 < F_f < 0.1$. The exact range of F_f values that correspond to predicted n values coincident with those observed in the field is dependent on C_i/α. This range of freshwater Froude numbers is consistent with typical values observed in the field (see section 6 and Fig. 11b). Furthermore, typical values of C_i are on the order of 10^{-4} (Sorgard et al. 1990; MacDonald and Geyer 2004), and we see in Fig. 5 that C_i/α values as large as 10 significantly modify n. Therefore, mean bottom slopes as small as 10^{-5} are enough to reduce n below the canonical value of 2 to 2.5 derived from the theory of Schijf and Schönfeld (1953). This suggests that slope effects may explain the deviation of observed length–discharge relationships in salt wedge estuaries from the flat estuary solution.

Unlike in the flat, prismatic channel solution presented above, n is now a function of the parameter C_i/α. Prediction of this parameter is complicated by the variation of channel bottom slope about the mean value. The local variation in α is comparable to the uncertainty in C_i. However, model runs using the full bathymetric profile of the Merrimack River, discussed in section 6b, suggest that the model is insensitive to variations in bottom slope about the mean, when compared to the results obtained assuming a constant bottom slope. More significant is the dependence on C_i, which is both an uncertain parameter and a global parameter within the model, affecting the entire intrusion and modifying the dependence of L on Q. This makes it difficult to predict the exact value of n a priori and therefore to use the observed length–discharge relationship to diagnose the dynamic regime. However, we show in section 6 that this solution is a significant improvement over the results of Schijf and Schönfeld (1953).

5. Solution for flat and sloped estuaries of converging width

We next consider the solution for intrusion length in an exponentially converging estuary, that is, an estuary of landward-decreasing width that can be described by

$$b(x) = b_\infty + (b_0 - b_\infty)e^{x/a}, \tag{23}$$

where $b(x)$ is the width at a given location x in the channel, b_∞ is the uniform width in the channel upstream of the estuary, b_0 is the width of the channel at the mouth, and a is the convergence length. This configuration is shown schematically in Fig. 2 (bottom right). Salt wedges typically occur in coastal plain estuaries (Valle-Levinson 2011), where an exponential equilibrium profile often exists (Savenije 2005). In section 6b, we compare our model to data for the Duwamish and Merrimack River estuaries. The Duwamish is a highly urbanized and channelized estuary and so is not effectively described by a simple exponential model. However, the Merrimack, outside of an expansive tidal embayment, is described very effectively by an exponential profile of the above form ($R = 0.64$, fit not shown). In both cases, we will begin by examining a uniform width solution and then incorporate a simplified width model based on the observed geometry of the estuary.

We nondimensionalize this width profile by dividing by the width at the mouth b_0:

$$b_*(x_*) = \frac{1}{R_c} + \left(1 - \frac{1}{R_c}\right) e^{x_*/a_*}, \tag{24}$$

where we have defined the convergence ratio $R_c = b_0/b_\infty$, which is the ratio of the width at the mouth to that in the upstream river, and the nondimensional convergence length $a_* = C_i a/h_S$, which is nondimensionalized in the same manner as x_* and L_*. These parameters indicate the magnitude (R_c) and rate ($1/a_*$) of exponential convergence.

a. *Existence of hydraulic solutions in a converging estuary*

A subcritical hydraulic solution for an arrested saline intrusion in a converging estuary does not necessarily exist. Rearranging Eq. (13) produces a cubic equation relating h_{1*} to $\Delta H'_*$:

$$h_{1*}^3 - \Delta H'_* h_{1*}^2 + \frac{1}{2}\frac{F_f^{4/3}}{b_*^2} = 0. \tag{25}$$

This relationship indicates that there is a minimum allowable value of $\Delta H'_*$, equal to $3/2b_*^{2/3}$, that is a function of the local width $b_*(x_*)$ and therefore position x_*. This is the nondimensional local critical buoyant hydraulic head anomaly $\Delta H'_{*_c}$. If the value of $\Delta H'_*$ falls below the local value of $\Delta H'_{*_c}$, then no subcritical hydraulic solution in which the mouth acts as control exists. If the mouth acts as control, the value of $\Delta H'_*(x_* = 0) = \Delta H'_{*_c}(x_* = 0)$. In a converging estuary, the local value of the critical buoyant hydraulic head anomaly increases upstream as the width decreases because $\Delta H'_{*_c} \sim b_*^{-2/3}$. Thus, $\Delta H'_*$ must at least initially increase upstream at a faster rate than $\Delta H'_{*_c}$ if a solution is to exist in which the mouth acts as control. If the solution considered were frictionless, $\Delta H'_*$ would be conserved and no solution could exist in a converging channel. However, if friction at the interface is considered, $\Delta H'_*$ increases upstream at the rate given by Eq. (15):

$$-\frac{d\Delta H'_*}{dx_*} = \frac{F_f^{4/3}}{b_*^2 h_{1*}^3}\left(1 + \frac{h_{1*}}{h_{2*}}\right),$$

where the negative sign is included because we are interested in the rate of increase upstream, but the positive x_* direction is taken to be downstream. Therefore, a solution for a subcritical salt wedge controlled at the mouth can exist only if interfacial friction is considered.

It is not possible to determine all necessary and sufficient conditions for existence of a hydraulic solution because the solution will fail anywhere that $\Delta H'_*$ falls below $\Delta H'_{*_c}$, but $\Delta H'_*$ is a property of the solution that cannot be determined a priori. We may, however, formulate a necessary condition for existence based on the behavior of the solution at the mouth. The specific head anomaly is equal to the local critical specific head anomaly at the control (by definition). Thus, the upstream rate of increase of $\Delta H'_*$ at the mouth, given by

$$-\left(\frac{d\Delta H'_*}{dx_*}\right)_{x_*=0} = \frac{1}{F_f^{2/3}(1 - F_f^{2/3})}, \tag{26}$$

must exceed the rate of increase $\Delta H'_{*_c}$ at the same location, given by

$$-\left(\frac{d\Delta H'_{*_c}}{dx_*}\right)_{x_*=0} = -\frac{d}{dx_*}\left(\frac{3}{2b_*^{2/3}}\right)_{x_*=0} = \left(\frac{db_*}{dx_*}\right)_{x_*=0}. \tag{27}$$

From Eq. (24), we find that

$$\left(\frac{db_*}{dx_*}\right)_{x_*=0} = \frac{1}{a_*}\left(1 - \frac{1}{R_c}\right). \tag{28}$$

Combining Eqs. (26)–(28), and requiring that $\Delta H'_*$ increase at a rate faster than $\Delta H'_{*_c}$, we find a necessary (though not sufficient) condition for existence of a hydraulic arrested salt wedge solution in an exponentially converging estuary:

$$\frac{a_*}{1 - R_c^{-1}} > F_f^{2/3}(1 - F_f^{2/3}). \tag{29}$$

The uniform width solution is obtained when the convergence ratio $R_c = 1$ or when the nondimensional convergence length $a_* \to \infty$. In either case, the left-hand side of Eq. (29) goes to infinity, consistent with the fact that a hydraulic solution always exists in the uniform width case. The right-hand side has a maximum of ¼ at $F_f = 1/(2\sqrt{2}) \approx 10^{-0.452}$. We anticipate that there will be regions where a hydraulic solution does not exist centered on $F_f = 10^{-0.452}$ for sufficiently small convergence lengths and/or sufficiently large convergence ratios. This will be examined in the following section.

b. *Length–discharge relationship*

We now explore the length–discharge relationship in flat and sloped converging estuaries. We recall that, having now introduced the convergence ratio R_c and nondimensional convergence length a_*, and suppressing the dependence on $\Delta\rho/\rho_2$, L_* is a function of F_f, C_i/α, R_c, and a_*.

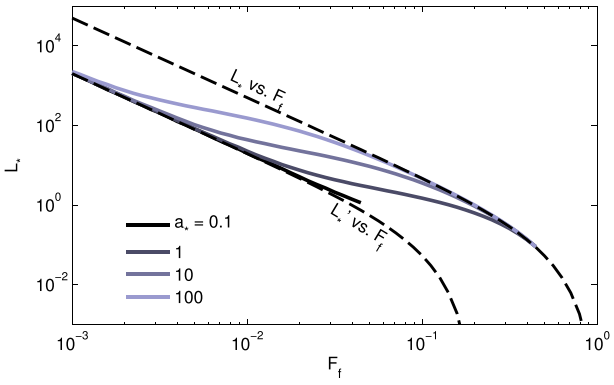

FIG. 6. Intrusion length in a flat channel ($\alpha = 0$) with varying convergence length a_* and constant convergence magnitude $R_c = 5$. The black dashed lines show the asymptotic solutions discussed in the text. All solid curves are colored based on the value of the nondimensional convergence length a_*.

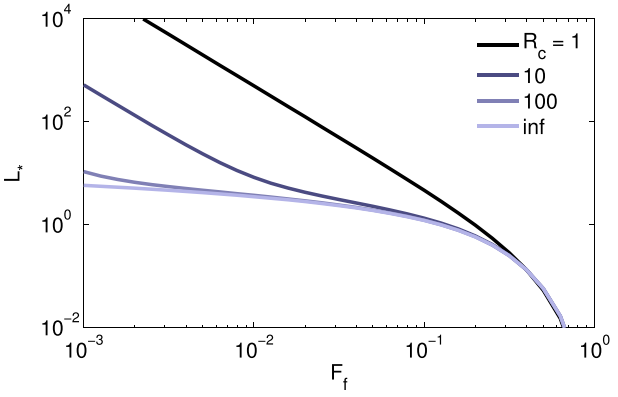

FIG. 7. Intrusion length in a flat channel ($\alpha = 0$) with constant convergence length $a_* = 1$ and variable convergence magnitude R_c. All solid curves are colored based on the value of the convergence ratio R_c. The $R_c = 1$ line corresponds to the Schijf and Schönfeld (1953) solution.

1) FLAT ESTUARY

The solution for intrusion length in a flat, converging estuary is shown in Figs. 6 and 7. In Fig. 6, we compare the flat, prismatic estuary solution (labeled "L_* vs. F_f"); four solution curves with $R_c = 5$ and values of a_* ranging from 0.1 to 100 as labeled; and a modified version of the flat, prismatic estuary solution (labeled "L'_* vs. F_f"). The value of L'_* is obtained based on a modified freshwater Froude number

$$F'_f = \frac{Q}{b_\infty \sqrt{g' h_S^3}} = \frac{b_0}{b_\infty} \frac{Q}{b_0 \sqrt{g' h_S^3}} = R_c F_f \qquad (30)$$

using Eq. (21), the solution for L_* in a flat estuary of uniform width developed by Schijf and Schönfeld (1953). The solution asymptotes to these two bounding solutions, corresponding to uniform estuaries of width equal to the width at the mouth and in the river, for high and low freshwater Froude numbers, respectively. The transition between the bounding solutions occurs when L_* is roughly between 1 and 10 times a_*. This is discussed extensively in section 6a below and shown schematically in Fig. 10b. The gaps on each of the curves correspond to regions where a hydraulic solution does not exist. The region of nonexistence shrinks for increasing nondimensional convergence length a_*, as Eq. (29) would predict. However, Eq. (29) predicts existence where it was found that hydraulic solutions do not exist. This is an indication that it indeed is not a sufficient criterion to guarantee existence, as discussed above.

Figure 7 shows the solution for a constant value of the nondimensional convergence length $a_* = 1$ and different values of the convergence ratio R_c. We show the uniform width Schijf and Schönfeld (1953) solution, which corresponds to $R_c = 1$, and the solution curves for $R_c = 10$ and 100; these curves display the same asymptotic behavior as observed in Fig. 6. We have also plotted the solution obtained in the limit that $R_c \to \infty$, which corresponds to a width at the mouth that is infinitely larger than that in the upstream river. We see that the finite R_c length–discharge relationships follow the $R_c \to \infty$ curve in the transition region. By investigating the behavior of infinite R_c solutions with different values of a_* (figure not shown), we found that n is nearly independent of a_* and $O(0.1)$ for $F_f < 10^{-3}$. This indicates that convergence by itself in a flat estuary could potentially account for the discrepancy between the Schijf and Schönfeld (1953) solution and observations. However, topography data from the Duwamish and Merrimack Rivers, examined in section 6b below, as well as from the Fraser River estuary indicate values of R_c on the order of 5 to 10. In this case, though n is reduced in the transition region, it remains $O(1)$, and the reduction is not enough to account for the discrepancy.

2) SLOPED ESTUARY

Figures 8 and 9 show the effects of varying R_c and a_*, respectively, on the intrusion length when the bottom slope α is nonzero and C_i/α is therefore finite. In Fig. 8, the nondimensional convergence length a_* is held constant at 1 while the convergence ratio R_c is varied between 1 and 10. We expect from above that the modification of the solution curve due to contracting width effects occurs when $L_* > a_*$. Thus, we anticipate that significant modification of the solution curve will occur only when the maximum possible value of L_*, C_i/α, is greater than a_*. Additionally, since the limiting value of L_* is independent of width, the effects of variable width

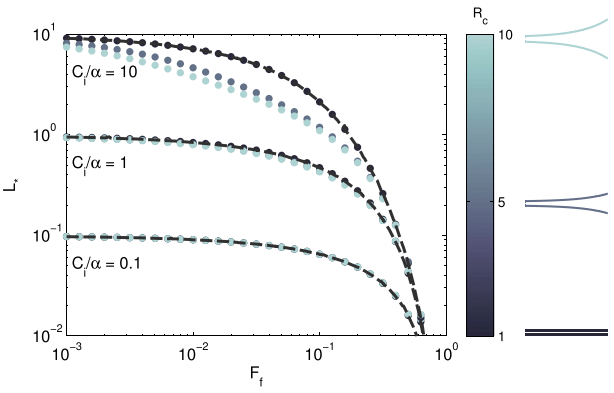

FIG. 8. Intrusion length in a sloped channel ($\alpha \neq 0$) with constant convergence length $a_* = 1$ and variable convergence magnitude R_c. The dashed black lines indicate the prismatic channel solution (from Fig. 5). All converging solution curves (dots) are colored based on the value of the convergence ratio R_c. Illustrations to the right of the figure indicate how the estuary shape changes as R_c is modified and a_* is held constant.

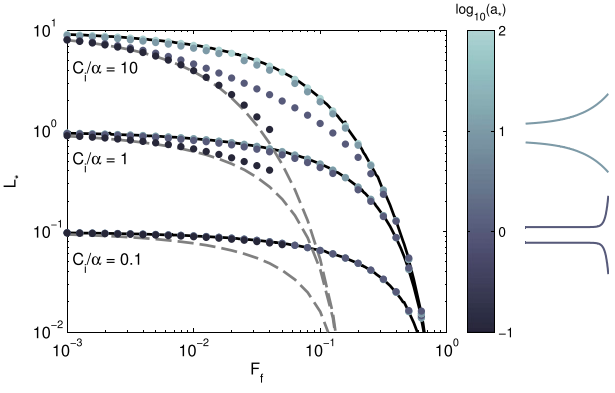

FIG. 9. Intrusion length in a sloped channel ($\alpha \neq 0$) with varying convergence length a_* and constant convergence magnitude $R_c = 5$. The solid black and dashed gray lines indicate the asymptotic prismatic channel solutions. The black lines correspond to uniform width solutions with $b = b_0$, the width at the mouth; the dashed gray lines correspond to uniform width solutions with $b = b_\infty$, the width in the upstream river. All converging solution curves (dots) are colored based on the value of a_*. Illustrations to the right of the figure indicate how the estuary shape changes as a_* is modified and R_c is held constant.

should become less apparent as $L_* \to C_i/\alpha$, that is, as $F_f \to 0$. This is precisely what is observed in Fig. 8. Noticeable deviation of L_* from the constant width values occurs only for the curve for which $C_i/\alpha > a_*$ ($C_i/\alpha = 10$ and $a_* = 1$). The deviation associated with R_c also decreases with decreasing F_f, as anticipated, and increases with R_c, as would also be expected. The magnitude of the effect of converging width on the intrusion length is highly dependent on the geometry of the estuary, in particular on how the slope-limited value of the intrusion length compares to the width convergence length of the estuary. Synthesizing our observations, we conclude that exponential estuary convergence has a significant impact on intrusion length only when $(C_i/\alpha)/a_* = h_S/(\alpha a) > 1$.

In Fig. 9, as in Fig. 6, R_c is held constant at 5 while a_* is varied between 0.1 and 100. As we would expect, the larger the ratio of C_i/α to a_*, the greater the effect of the variable width. Additionally, the effect of the variable width becomes less apparent at lower values of F_f as the slope-limiting mechanism becomes more important. Depending on how greatly C_i/α exceeds a_*, the predicted intrusion length may deviate by as much as an order of magnitude from the uniform width value. However, the intrusion length is bounded by that which would be obtained in an estuary of uniform width b_∞. This is represented by the gray dashed lower bounding curves for each set of curves corresponding to a different value of C_i/α in Fig. 9. We observe that width convergence can indeed significantly affect the value of n when the estuary slope is nonzero. However, we note from Fig. 8 that, even when the effects of width convergence are most pronounced, they are still secondary to those of slope limitation on the value of n. We therefore conclude that mean bottom slope likely has the more significant effect on n in real salt wedge estuaries.

6. Discussion

We have developed solutions for the dependence of intrusion length in a highly stratified salt wedge estuary on river discharge for estuaries with nonzero bottom slope and converging width. Our solutions indicate that 1) nonzero bottom slope strongly modifies the magnitude of dependence of L on Q (characterized by the value of n in the relationship $L \sim Q^{-n}$) for even modest bottom slopes, 2) there is a transition region where convergence tends to decrease n in both flat and sloped estuaries, 3) within the typical parameter space, the influence of nonzero bottom slope is greater than the influence of convergence on the length–discharge relationship in a salt wedge estuary, and 4) the reduction of n in the sloped estuary solutions is enough to account for the deviation of observations from the theory for flat, prismatic channels developed by Schijf and Schönfeld (1953). In section 6b, we will assess whether our solution is consistent with available data.

a. *Slope limitation and estuary convergence*

The slope-limitation mechanism is described in section 4 and is shown schematically in Fig. 10a. Unlike in the flat estuary case, there is a finite limit to the distance

the salt wedge can penetrate upstream. As the discharge approaches zero, the thickness of the salt wedge at the mouth approaches the shoreline depth, and the intrusion length approaches h_S/α. This corresponds to a limiting value of the nondimensional intrusion length $L_* = C_i/\alpha$. Physically, as the salt wedge intrudes into an estuary of nonzero mean bottom slope, the change in elevation of the pycnocline from mouth to toe is less than in a flat estuary. This corresponds to a smaller mean interfacial slope and therefore a weaker mean baroclinic pressure gradient forcing the upstream propagation than in the flat estuary case. Additionally, the reduced water depth results in reduced layer thicknesses and correspondingly enhanced friction. These mechanisms allow the slope-limitation mechanism to be felt over the entire parameter space and have such a strong impact on the value of n, decreasing it by an order of magnitude relative to the flat bottom case.

In our simplified model of a variable width estuary, in which we assumed the width decreased exponentially from its value at the mouth to a uniform value in the upstream river, we found that the solution for intrusion length as a function of discharge asymptotes between solutions based on the width at the mouth and the width in the upstream river. As illustrated in Fig. 10b, the transition zone between these two solutions was observed to lay between 1 and 10 convergence lengths landward of the mouth. For intrusion lengths less than the convergence length, the intrusion does not feel the change in width, behaving as if the channel width were constant and equal to the width at the mouth b_0. When the intrusion length is greater than 10 convergence lengths, the intrusion feels only the width of the upstream river b_∞. In between, it transitions between the two asymptotic solutions, as observed in Figs. 6 and 9. Within the transition zone, the value of n is decreased in both flat and sloped estuaries.

We can combine these two observations to determine a criterion for when width convergence has an effect on intrusion length. The salt wedge can only penetrate a distance h_S/α into the estuary. Convergence effects only become relevant when $L > a$. Therefore, convergence alters intrusion length only if $h_S/(\alpha a) > 1$. This is apparent in Figs. 8 and 9, in which we see there is no deviation of the converging estuary solution from the uniform width solution when $a_* = C_i a/h_S < C_i/\alpha$.

b. Comparison of L versus Q to real estuaries

In this section, we compare the sloped estuary solution for intrusion length to numerical data from an extensively validated realistic numerical model of the Merrimack River estuary (Ralston et al. 2010) and field data from the Duwamish River estuary (McKeon et al. 2014, manuscript submitted to *Estuaries Coasts*). In both cases, we begin with a sloped uniform width model and then examine the influence of a simplified version of the observed width profile on the solution. Both estuaries are observed to be salt wedges (Ralston et al. 2010; McKeon et al. 2014, manuscript submitted to *Estuaries Coasts*). Data for intrusion length, tidal amplitude, and river discharge from a Finite Volume Ocean Costal Model (FVCOM) of the Merrimack was provided by Dr. D. K. Ralston. A detailed description of the model can be found in Ralston et al. (2010). The intrusion length provided is the landwardmost location of the intersection of the 2-psu isohaline with the channel bottom. Maximum intrusion occurs soon after high water. Ideally, we would compare to intrusion length determined as the landwardmost extent of the point of

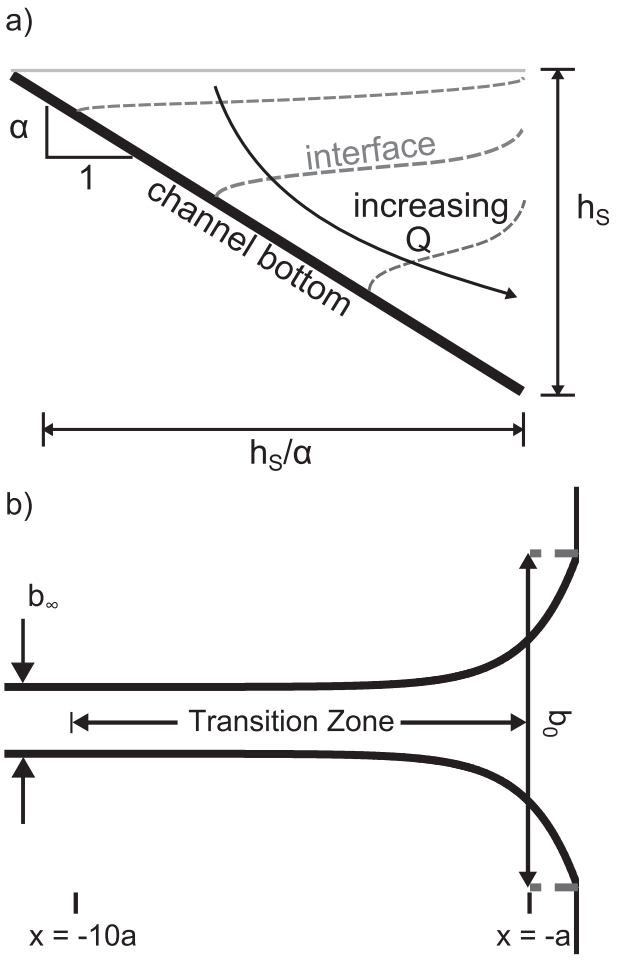

FIG. 10. (a) Schematic showing slope-limited salt wedge. (b) Schematic showing location of the transition zone. For $L < a$, the intrusion is set by the width at the mouth b_0. For $L > 10a$, the intrusion is set by the width in the upstream river b_∞. In between, the intrusion length transitions between these two asymptotic solutions.

maximum bottom salinity gradient, since our model predicts the structure of the pycnocline. Using the 2-psu isohaline instead introduces some error when comparing the numerical data to our model owing to the finite thickness of the density front in real estuaries. However, we assume that the extent of the salinity front is small compared to the intrusion length so that the associated error is small. We compare data for the smallest modeled tidal amplitude (2 m) to the hydraulic solution presented here to assess whether the hydraulic solution accurately characterizes the dependence of intrusion length on discharge. The lowest tidal amplitude was selected so that tidal effects, which are not considered here, are minimized.

Assuming the mouth acts as control, it is necessary to determine the width and depth at the mouth to calculate the freshwater Froude number. Based on bathymetric data provided for the Merrimack, the width of the estuary at the mouth is $b_0 = 320$ m, the mean bottom slope is 2.3×10^{-4}, and the shoreline depth is $h_S = 7.75$ m.

From these values of h_S and b_0, along with the discharges corresponding to the modeled salinity intrusions, we can determine the values of the freshwater Froude number $F_f = Q/b_0\sqrt{g'h_S^3}$, provided that we know the value of $\Delta\rho/\rho_2$. Given the uncertainty in the estuary-averaged top-to-bottom salinity difference at arrest, we allow the stratification to vary when finding a best fit of the hydraulic solution to the data and then confirm that this value is reasonable.

The values of $L_* = C_iL/h_S$ and C_i/α also depend on the value of C_i, which is found to be in the range $1(\times 10^{-4})$ to $5(\times 10^{-4})$ (Sorgard et al. 1990; MacDonald and Geyer 2004). The model is fit to the data by systematically varying C_i and $\Delta\rho/\rho_2$ and determining the values of C_i and $\Delta\rho/\rho_2$ for which the sum of the normalized squared residuals is minimized. In finding the best fit, C_i is allowed to vary over the range 10^{-6} to 10^{-2} in order to robustly test if the model will settle on a value falling within the typically observed range, and $\Delta\rho/\rho_2$ over the range 0.01 to 0.023. The stratification value represents an average over different discharges and longitudinally through the salt wedge at the moment of arrest; therefore, it is not clear a priori what value is appropriate. The goodness of fit (assessed by visual inspection and normalized absolute error) and the values of $\Delta\rho/\rho_2$ and C_i provide an indication of whether or not the variable slope hydraulic solution for intrusion length accurately describes the data. The values of C_i and $\Delta\rho/\rho_2$ obtained are 4×10^{-4} and 0.013, respectively. That C_i was allowed to vary over four orders of magnitude and converged to a value within the typically observed range suggests that the hydraulic model accurately describes the behavior of the system. The value of $\Delta\rho/\rho_2 = 0.013$ corresponds to a top-to-bottom salinity difference of 17 psu, roughly midrange between oceanic (30 psu) and freshwater salinity. In reality, the value of $\Delta\rho/\rho_2$ will vary with location in the salt wedge and river discharge, but these complexities are neglected here. This fit produces a mean normalized absolute error of 48%; however, much of this error is due to the underprediction of intrusion length near the mouth in the vicinity of the tidal embayment (discussed further below). Excluding these points, the normalized error is 30%. The graphical comparison of the numerical model data to the prediction of the hydraulic model, along with the corresponding solution for a flat, prismatic estuary (Schijf and Schönfeld 1953), is shown in Fig. 11b. The hydraulic-model-incorporating bottom slope is a significant improvement over the Schijf–Schönfeld solution; the model predicts the correct order of magnitude for the salinity intrusions when the freshwater Froude number is below ~0.3 (the majority of the data), as well as for the magnitude of dependence of salinity intrusion on discharge, characterized by n, the slope of the L_*–F_f curve in logarithmic space. In contrast, the Schijf–Schönfeld solution predicts salinity intrusions that are as much as three orders of magnitude greater than the numerical model data and a value of n that is an order of magnitude larger than observed.

In Fig. 11b, we see that the (uniform width, uniform slope) hydraulic solution underpredicts intrusion length for $F_f > \sim 0.2$ and overpredicts intrusion length for $F_f < \sim 0.1$. Possible reasons for the failure of this simple hydraulic model include the effects of variable width, local variations in the channel bottom elevation about the mean bottom slope, the variation of mean top-to-bottom stratification with discharge, tides, and the inapplicability of the assumptions of the hydraulic theory (e.g., the flow is not quasi steady and/or one-dimensional, there is not a predominantly two-layer flow structure, the pycnocline occupies a significant portion of the water column). Also shown in Fig. 11b (dash–dotted line) is the hydraulic model solution incorporating a variable width profile. From the constriction landward, the variation in width allows the saline intrusion to penetrate further up-estuary than it would have otherwise. This suggests that some of the increased intrusion at higher discharges may be explained by the effects of variable width. However, within and seaward of the embayment, the predicted intrusion length is now smaller than predicted by the uniform width model. Thus, it is unlikely that variable width explains the divergence for high discharges. The normalized absolute error is 50%, nearly unchanged from the uniform width model.

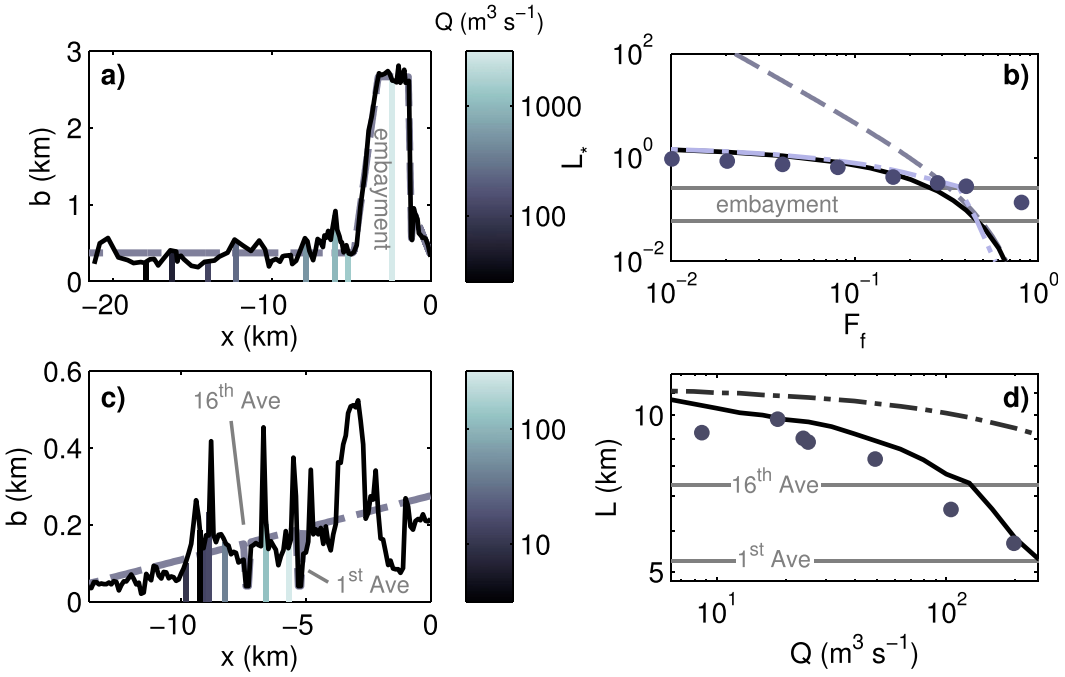

FIG. 11. Top-width profiles of the (a) Merrimack and (c) Duwamish (solid black), salt wedge toe locations as function of discharge (solid, colored), and simplified width profile used in analysis (gray, dashed). (b) Comparison of Merrimack numerical model data (Ralston et al. 2010, gray-blue dots) to flat, prismatic estuary solution (Schijf and Schönfeld 1953, dashed gray line) and current solution without (solid black line) and with (light blue dash–dotted line) variable width. (d) Comparison of Duwamish field data (gray-blue dots) to the current solution assuming either control at the mouth and constant width (dash–dotted gray) or variable width and control location (solid black).

The tendency for the hydraulic model to overpredict intrusion length for lower discharges and underpredict intrusion length for higher discharges would be consistent with stratification ($\Delta\rho/\rho_2$) that increased with discharge. However, the solution curves corresponding to a top-to-bottom salinity difference of 5 and 30 were calculated (not shown), and it was found that the corresponding differences in predicted intrusion length are relatively small compared to the difference between the numerical data and prediction of the hydraulic model. The hydraulic model was also run with the true channel bottom elevation profile (not shown), but the results were not significantly different from the solution obtained using a constant slope and did not explain the deviation of the hydraulic prediction from the numerical model data.

Underprediction of intrusion length at high discharges and overprediction at low discharges is also consistent with the effects of tidal forcing. We would anticipate that, at high discharges, when the intrusion length that would be obtained under the river discharge alone is small, tidal advection during the flood will force the intrusion far past this equilibrium point, whereas at low discharges, when the intrusion length under the action of the river discharge alone is large, the salt wedge will not have time to reach the equilibrium point with the river within half of the tidal period. This is consistent with the behavior observed in Fig. 11b. The good performance of this hydraulic solution in predicting the intrusion length suggests that the behavior of L with Q is in fact consistent with the previously observed hydraulic behavior of these estuaries.

The predicted intrusion length was also compared to field data taken in the Duwamish (McKeon et al. 2014, manuscript submitted to *Estuaries Coasts*). McKeon et al. (2014, manuscript submitted to *Estuaries Coasts*) define intrusion length as the landwardmost point with a top-to-bottom salinity difference greater than five. This presumably gives a better indication of the location of the toe than the 2-psu isohaline. The intrusion lengths have been interpolated to one-quarter of the way through flood tide (hereafter referred to as ''quarter flood'') because this was the most reliably sampled phase of the tide. The model introduced here predicts the maximum intrusion length at the time of arrest before lower-layer reversal. However, the comparison of the model to this data will still give an idea of whether or not it is able to predict the magnitude of dependence of intrusion length on discharge accurately.

Figure 11d shows the field data, this time in terms of L and Q—not L_* and F_f. Dimensional variables are

plotted because we consider a hydraulic model with variable control points. We find that a uniform width solution assuming control at the mouth, similar to the solution applied to the Merrimack, overpredicts intrusion length by as much as 4 km, larger than the 3.6-km tidal excursion of the salt wedge toe reported by Dawson and Tilley (1972), and does not accurately reproduce the observed dependence on discharge. We hypothesize that this is because the flow is not controlled at the mouth under low discharge conditions and that the relevant control point may vary between the mouth and significant flow constrictions associated with the 1st and 16th Avenue Bridge piers, located at river kilometers 5.2 and 7.3, respectively (Fig. 11c).

To test this, we modified the model to include a linearly converging width profile superimposed with the two pier constrictions (Fig. 11c) and allowed the control location to vary. The control is assumed to be the landwardmost potential control point that is accessible by the intrusion. Thus, an iterative method of determining the location of control, wherein the seawardmost control is assumed and the solution is integrated landward until either the toe or the next potential control point is reached, is implemented. We could also have obtained a solution by assuming that a control was not activated when it became accessible—that is, by assuming that intrusions extending past the more landward 16th Avenue Bridge pier were still controlled at the 1st Avenue Bridge pier. This creates some ambiguity in the solution; however, evidence is presented in McKeon et al. (2014, manuscript submitted to *Estuaries Coasts*) suggesting that the 16th Avenue Bridge pier does indeed control the flow when the lower layer extends that far landward. The variable control point model consistently overpredicts the intrusion length, as we would expect because the data are taken at quarter flood, and accurately reproduces the value of $n \approx 0.2$, again an order of magnitude smaller than the canonical value from Schijf and Schönfeld (1953) (McKeon et al. 2014, manuscript submitted to *Estuaries Coasts*). Note that for both of the hydraulic models of the Duwamish we chose typical values of the interfacial drag coefficient and density anomaly—$C_i = 10^{-4}$ (Sorgard et al. 1990; MacDonald and Geyer 2004) and $\Delta\rho/\rho_2 = 0.02$, roughly corresponding to the ocean-basin salinity difference of 28 psu (McKeon et al. 2014, manuscript submitted to *Estuaries Coasts*)—rather than fitting the data. Because the data come from quarter flood, a fit to the data produces unreasonably high values of C_i [$O(10^{-3})$] to account for the fact that the intrusions have not reached the arrest point.

When mean bottom slope is included, the predictions of the hydraulic model are consistent with field observations in the Duwamish and a well-validated numerical model of the Merrimack, which are both observed to behave as salt wedge estuaries (Ralston et al. 2010; McKeon et al. 2014, manuscript submitted to *Estuaries Coasts*). This potentially eliminates the need to appeal to more complex momentum balances and scalings for the intrusion length based on the dominance of tidal or exchange flux in estuaries that otherwise behave hydraulically, as is suggested by some authors (e.g., Ralston et al. 2010; Lerczak et al. 2009). This is a significant result insofar as the behavior of L with Q is to be used as a diagnostic criterion for the dynamics of an estuary. Additionally, the potential resolution of the uncomfortable disparity between the clearly hydraulic behavior of salt wedge estuaries and the predictions of hydraulic theory is a significant result in itself.

7. Conclusions

We have found that even modest bottom slopes [$O(10^{-5})$] significantly reduce the magnitude of dependence of intrusion length on discharge for freshwater Froude numbers $F_f \sim O(0.1)$ or smaller, owing to the finite value of the maximum intrusion length in a sloped estuary. The solution for a sloped estuary of uniform width presented here predicts exponents n in a relationship of the form $L \sim Q^{-n}$ in the observed range (0.2–0.6) for freshwater Froude numbers roughly in the range 0.01–0.1 (Figs. 5, 11b). This solution shows that the value of n is highly dependent on C_i, an uncertain parameter, making it difficult to predict its value a priori. However, the solution presented here is a significant improvement over the solution of Schijf and Schönfeld (1953), giving an order of magnitude improvement in the prediction of n.

In an estuary of convergence length a, we find that the effect of convergence on the length–discharge relationship becomes significant only for intrusion lengths $L > a$. Convergence decreases the intrusion length from the value that would be obtained for the same discharge in an estuary of uniform width equal to the width at the mouth (Figs. 6, 8, 9). The intrusion length is bounded by the solutions for uniform width estuaries of width equal to that at the mouth of the estuary and in the upstream river (Figs. 6, 9). Within the transition zone ($a < L < 10a$), convergence tends to decrease the magnitude of n in both flat and sloped estuaries (Figs. 6, 9). Convergence can strongly modify the particular value of n in an estuary, but nonzero slope is the more significant influence for reasonable bottom slopes $C_i/\alpha \leq 10$ and convergence ratios $R_c \leq 10$.

The results from our comparison with field data from the Duwamish and numerical data from the Merrimack indicate that the solution presented here is consistent with observed values of n in salt wedge estuaries. The actual intrusion length is not captured as accurately by the simple hydraulic solution owing to complications due to topography, tides, and other influences. However, these results suggest that the discrepancy between observed values of n and the canonical values of 2–2.5 is consistent with the influence of geometry on the hydraulic solution, primarily the effect of nonzero mean bottom slope, potentially eliminating the need to appeal to other dynamic influences or regimes to resolve this discrepancy.

Acknowledgments. The authors thank M. A. McKeon for helpful feedback and discussions and for providing field data, Dr. D. K. Ralston for providing numerical data, and Dr. M. P. Lamb for helpful discussions. This work was funded by National Science Foundation Grant OCE-1233068. A.R.H.D. is grateful for support from the Allan and Inger Osberg Endowed Professorship.

REFERENCES

Armi, L., 1986: The hydraulics of two flowing layers with different densities. *J. Fluid Mech.*, **163**, 27–58, doi:10.1017/S0022112086002197.

——, and D. M. Farmer, 1986: Maximal two-layer exchange through a contraction with barotropic net flow. *J. Fluid Mech.*, **164**, 27–51, doi:10.1017/S0022112086002458.

Chatwin, P. C., 1976: Some remarks on the maintenance of the salinity distribution in estuaries. *Estuarine Coastal Mar. Sci.*, **4**, 555–566, doi:10.1016/0302-3524(76)90030-X.

Chow, V. T., 1959: *Open-Channel Hydraulics.* McGraw-Hill, 690 pp.

Dawson, W. A., and L. J. Tilley, 1972: Measurement of salt-wedge excursion distance in the Duwamish River estuary, Seattle, Washington, by means of the dissolved-oxygen gradient. USGS Water Supply Paper 1873-D, 27 pp. [Available online at https://pubs.er.usgs.gov/publication/wsp1873D.]

Geyer, W. R., and D. M. Farmer, 1989: Tide-induced variation of the dynamics of a salt wedge estuary. *J. Phys. Oceanogr.*, **19**, 1060–1072, doi:10.1175/1520-0485(1989)019<1060:TIVOTD>2.0.CO;2.

——, and D. K. Ralston, 2011: The dynamics of strongly stratified estuaries. *Water and Fine Sediment Circulation*, E. Wolanski, and D. McLusky, Eds., Vol. 2, *Treatise on Estuarine and Coastal Science*, Elsevier, 37–51, doi:10.1016/B978-0-12-374711-2.00206-0.

——, and P. MacCready, 2014: The estuarine circulation. *Annu. Rev. Fluid Mech.*, **46**, 175–197, doi:10.1146/annurev-fluid-010313-141302.

Harleman, D. R. F., 1961: Stratified flow. *The Handbook of Fluid Dynamics*, V. L. Streeter, Ed., McGraw-Hill, 26-1–26-21.

Keulegan, G. H., 1957: Form characteristics of arrested saline wedges. NBS Rep. 5482, National Bureau of Standards, 75 pp.

——, 1966: The mechanism of an arrested saline wedge. *Estuary and Coastline Hydrodynamics*, A. T. Ippen, Ed., McGraw-Hill, 546–574.

Lamb, M. P., J. A. Nittrouer, D. Mohrig, and J. Shaw, 2012: Backwater and river plume controls on scour upstream of river mouths: Implications for fluvio-deltaic morphodynamics. *J. Geophys. Res.*, **117**, F01002, doi:10.1029/2011JF002079.

Lerczak, J. A., W. R. Geyer, and D. K. Ralston, 2009: The temporal response of the length of a partially stratified estuary to changes in river flow and tidal amplitude. *J. Phys. Oceanogr.*, **39**, 915–933, doi:10.1175/2008JPO3933.1.

MacCready, P., and N. S. Banas, 2011: Residual circulation, mixing, and dispersion. *Water and Fine Sediment Circulation*, E. Wolanski, and D. McLusky, Eds., Vol. 2, *Treatise on Estuarine and Coastal Science*, Elsevier, 75–89, doi:10.1016/B978-0-12-374711-2.00205-9.

MacDonald, D. G., and W. R. Geyer, 2004: Turbulent energy production and entrainment at a highly stratified estuarine front. *J. Geophys. Res.*, **109**, C05004, doi:10.1029/2003JC002094.

Monismith, S. G., W. Kimmerer, M. T. Stacey, and J. R. Burau, 2002: Structure and flow-induced variability of the subtidal salinity field in northern San Francisco Bay. *J. Phys. Oceanogr.*, **32**, 3003–3019, doi:10.1175/1520-0485(2002)032<3003:SAFIVO>2.0.CO;2.

Pratt, L. J., 1986: Hydraulic control of sill flow with bottom friction. *J. Phys. Oceanogr.*, **16**, 1970–1980, doi:10.1175/1520-0485(1986)016<1970:HCOSFW>2.0.CO;2.

Ralston, D. K., W. R. Geyer, and J. A. Lerczak, 2010: Structure, variability, and salt flux in a strongly forced salt wedge estuary. *J. Geophys. Res.*, **115**, C06005, doi:10.1029/2009JC005806.

Savenije, H. H. G., 2005: *Salinity and Tides in Alluvial Estuaries.* Elsevier Science, 208 pp.

Schijf, J. B., and J. C. Schönfeld, 1953: Theoretical considerations on the motion of salt and fresh water. *Proc. Minnesota Int. Hydraulic Convention*, Minneapolis, MN, University of Minnesota, 321–333.

Sorgard, E., T. Martinsen, and E. Aas, 1990: Drag coefficient at a stationary salt wedge. *J. Geophys. Res.*, **95**, 7337–7345, doi:10.1029/jc095ic05p07337.

Valle-Levinson, A., 2011: Classification of estuarine circulation. *Classification of Estuarine and Nearshore Coastal Ecosystems*, E. Wolanski, and D. McLusky, Eds., Vol. 1, *Treatise on Estuarine and Coastal Science*, Elsevier, 75–86, doi:10.1016/B978-0-12-374711-2.00106-6.

Ward, P., 1976: Seasonal salinity changes in the Fraser River estuary. *Can. J. Civ. Eng.*, **3**, 342–348, doi:10.1139/l76-031.